Freie Universität Berlin
Department of Physics
Arnimallee 14
14195 Berlin

WS 2011/12

Advanced Lab Course for Master Students
Report

Ma6 - Atomic Force Microscopy

Stefanie Kreft
kreft@physik.fu-berlin.de

Samuel Sanchez Viveros
sanchez@physik.fu-berlin.de

Pietro Cataldi
devilvespa_85@libero.it

December 31, 2011

Tutor: Ch. Lotze

Contents

1. Theoretical Background

The Atomic Force Microscope (AFM, 1986) permits, in contrasts to the Scanning Tunneling Microscope (STM; 1981), the study of conductive and non-conductive samples, such as insulators, semiconductors and electric conductors.
Whereas the STM images are a convolution of the electronic structure of tip and the surface, the AFM measures the force on the tip and thus the topography of the sample is determined.

1.1. Fundamentals

The AFM probes the surface with a sharp tip, which is only micrometers long and often less than 100Å in diameter. The tip is attached to the end of a cantilever, which is bended or deflected due to forces between the tip and the sample surface. This movement of the cantilever is detected with the help of a laser. The beam is focused onto the back of the free cantilever and then reflected. The reflection is detected by a position sensitive photodiode, which measures the bending of the cantilever precisely. The obtained data is used to generate a map of the surface.
The force acting between tip and sample consists of the superposition of different forces

$$F_{total} = F_{chem} + F_{vdW} + F_{electr.} + F_{magn.}, \tag{1.1.1}$$

with the chemical force, the van der Waals interaction, the electrostatic force and the magnetic force, which is only relevant for magnetic tips or samples and not used during the performed experiment.
For small distances, the total force is repulsive due to the Pauli interaction between the electronic shells of different atoms. The atoms are in contact. The van der Waals interaction is an attractive interaction between the permanent and temporary dipoles of tip and sample, valid for larger distances than the repulsive force. The range of the interaction is limited by the radius of the tip and the tip-sample distance. It can be approximated by a sphere in front of an infinitely extended surface $F_{vdW} = \frac{HR}{6d^2}$, where H is the Hamaker constant, R the radius of the tip and d the tip-sample distance.
The total force can be described by the Lennard-Jones potential $U_{chem} = 4\epsilon\left[(\frac{\sigma_0}{r})^{12} - (\frac{\sigma_0}{r})^{6}\right]$, where ϵ is the strength of the potential at minimum and σ_0 denotes distance at zero potential. Below this distance, the forces are repulsive.
The dependence of the total force on the tip-sample distance can be seen in fig. 1.1. Two distance regimes can be distinguished: The contact (cf. section 1.2) and the non-contact (cf. section 1.3) mode, the first referring to a regime with a repulsive, the second to

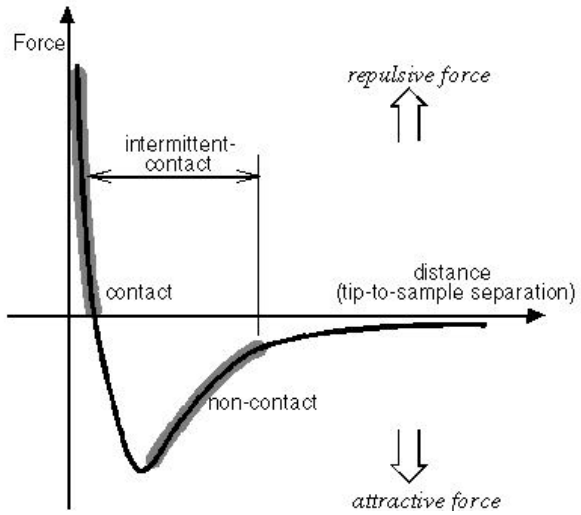

Fig. 1.1.: Dependence of the Force on the tip-sample distance [1]

a regime with attractive force. Two other forces have to be taken into account. The capillary forces, which is exerted by a thin layer of water that lays around the tip and applies an attractive force as well as the force exerted by the cantilever itself.

1.2. Contact Mode

For a tip-sample distance of only a few angstroms, the AFM is in the contact mode, also known as repulsive mode, where two more possibilities have to be distinguished. The constant-height and the constant-force mode. During the movement of the sample or tip, the contact force between tip and sample causes the cantilever to bend according to the changes in topography. For both measurements methods, the spring constant for the attachment between the tip and the cantilever has to be lower than the effective spring constant of the coupling between the atoms of the sample. This and the fact that the slope of the van der Waals curve is steep in the contact regime, therefore balancing most of the attempts to push the atoms closer together, leads to the bending of the cantilever rather than the movement of the sample atoms towards the surface. In constant-height mode, the topographic data can be directly gained from the spatial variation of the cantilever deflection, because the hight of the scanner is fixed.
In constant-force-mode, the deflection is used as input to a feedback circuit. Thereby, the scanner is moved in z-direction in such a way that the cantilever reflection and thus the total force applied to the sample, is constant. The topography image is generated from the motion of the scanner.

1.3. Non-Contact Mode

In the non-contact mode, the total force between tip and sample is very low. It can therefore be used to study soft or elastic samples that would be destroyed by other methods. It can also be used to examine a surface without contaminating it with the tip. But the low force and the fact that the cantilever has to be very stiff to prevent it from being pulled into contact mode, generates a low signal, which needs special means to be detected.
The cantilever is therefore excited via a piezo element to oscillate near its resonance frequency. When the tip is close enough to the sample, interaction between the tip and the sample can occur that force a shift of the resonance curve of the cantilever. If the frequency of the oscillation is fixed due to the external excitation, the amplitude of the oscillation changes. This can be detected by the photodiode. The equation of motion of the oscillation of the cantilever can be approximated by the movement of the damped harmonic oscillator with forced oscillation

$$m\ddot{z} + \gamma\dot{z} + kz = F_0 \cos(\omega t) + F_{total}, \tag{1.3.1}$$

where z is the tip-sample distance, γ the damping constant, k the spring constant of the cantilever and $F_0 \cos(\omega t)$ the excitation of the oscillation through piezoelectric element. The oscillation frequency is determined by the spring constant and the mass $\omega_0 = \sqrt{\frac{k}{m}}$. The interaction between tip and sample can be included in an effective spring constant

$$k_{eff} = k - \frac{\partial F_{total}}{\partial z}. \tag{1.3.2}$$

This effective constant shifts the resonance frequency with respect to free resonance. For small oscillation amplitudes, meaning that the variation of force gradient is small compared to amplitude, this shift can be approximated via $\Delta\omega_0 = -\frac{\omega_0}{2k}\frac{\partial F_{total}}{\partial z}$.
The gradient of the force can be approximated as

$$\frac{\partial F_{total}}{\partial z} = k\left(\frac{1 - 2a^2 + \sqrt{4\,Q^2\,(a^2-1)+1}}{2\,(Q^2 - a^2)}\right), \tag{1.3.3}$$

where $a = A_0/A$ is the amplitude of free resonance over the feedback amplitude and Q denotes quality factor of the cantilever [2].
For the measurements, the sample is mounted on a scanner, which allows the precise movement of the sample relative to the tip. The scanner consists of several piezo element, their movement is controlled by the application of an external voltage, but due to non-linearity effects, the piezo does not convert the applied voltage linearly into extension. Effects that have to be considered are explained in section 1.4.1 and the following.

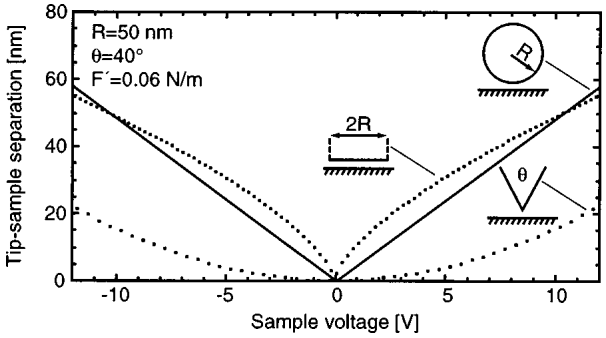

Fig. 1.2.: Theoretical expectations for the dependence of the tip-sample distance on the sample voltage for different shapes of the tips [3].

1.4. Electrostatic Forces

The electrostatic force between the tip and sample can be expressed as

$$F_{electr} = \frac{1}{2}\frac{\partial C}{\partial z}V_{eff}^2 \tag{1.4.1}$$

if tip and sample are assumed to form a capacitor. C is the capacitance, V_{eff} represents the entire applied voltage, which consists of the applied voltage V_{bias} and the contact potential $V_{CPD} = \frac{1}{e}(\phi_{sample} - \phi_{tip})$, which results from difference work functions of tip and sample.
The contact potential can be determined experimentally if the position of the tip on the sample and the height are fixed and the tip-sample voltage is detected as a function of the applied voltage. It will show a minimum when V_{bias} equals $-V_{CPD}$.
Another possibility is the determination of the force gradient, which depends on the geometry of the tip. If the force is held constant by the adjustment of the tip height, the latter will become a function of V_{bias}. Olsson et al. [3] determined typical curves for different tip shapes, which can be seen in fig. 1.2.

1.4.1. Non-Linearity

A piezoelectric element expands and contracts its length accordingly to the applied voltage. The strain s of the piezoelectric, which denotes the ratio between the variation of the length and the length ($s = \Delta l/l$), is assumed to vary linearly with the applied voltage $s = dE$, where E denoted the electric fields and d the strain coefficient. In reality, the relationship between strain and electric field is not linear.

Intrinsic Nonlinearity

The behavior of the extension of the piezoelectric element with the applied voltage performs a "s"-shaped increase. The ratio of the maximal derivation from the linearity to

this is called intrinsic non-linearity.
This effect leads to a distortion of the measurement grid, because the measured points are not equally spaced.
For measurement perpendicular to the surface, errors can occur as well. A calibration is needed to minimize the error.

Hysteresis

The piezoelectric elements also show a hysteretic behavior. The extension when the voltage is turned on differs from the extension when the voltage is turned off. Therefore the data is usually collected in one direction only to minimize errors.
Errors also occurs when the step-height of the surface is measured. The voltage needed for the movement upwards and downwards is different, resulting in an unequal height on the two sides of a step.

Creep

Another error occurs through an effect called creep. The reaction of the piezoelectric material is not instant, but occurs in two steps. The first one (x) happens in less than a millisecond, the second step occurs on a much longer scale (x_s). The creep is defined as $c = \Delta x_s / \Delta x$. Scans with different scan speed show the difference in the length scale. Therefore a calibration is needed.
Creep is especially of importance, when a certain area of interest is supposed to be measured. The movement to the location can be delayed and distort an already started measurement.

Aging

The strain coefficient changes exponentially with time and use. It depends on the alignment of the dipoles in the piezoelectric element. A piezoelectric element which is used regularly, shows a strong alignment of the dipoles, thereby increasing the strain coefficient. If the piezoelectric element is not used often, the dipoles are orientated randomly and the strain coefficient decreases.

Cross Coupling

Cross-Coupling describes the connection between the scan in x-y-direction and the z-direction, which can be caused by superposition of fields in the piezoelectric element.

2. Experimental Setup and Procedure

2.1. Experimental Setup

In this experiment an atomic force microscope (AFM) manufactured by NANOTEC was used. It consists of a chassis, which holds the piezo scanner and the sample holder; the head which contains the cantilever holder with the cantilever and the laser diode and the photodiode for detecting the movement of the cantilever. All these components contains several screws for coarse and fine adjustment of the components. The microscope was connected to a supply unit (*SPM Control System*) and could by controlled via an attached computer. The software used to control the microscope and to capture the pictures was provided by the manufacture in different versions. Throughout the experiment the version `WSxM 4.0 Beta 4.2` in the versions `1.0 (April 2000)` and `3.0 (July 2004)` was used.

2.2. Experimental Procedure

The laser had to be aligned in such a way, that it hits the tip of the cantilever and is then reflected into the center of the photodiode. This was first done with the head unmounted on the chassis and then mounted to the chassis with an inserted sample due to the high sensitive of the alignment. A thorough description of the alignment process is given in [4].

Before the measurements in non-contact mode could be started, the resonance frequency and the force constant of the tip hat to be determined. This can be done by the control software.

Measurements were performed with two different samples. The first sample consisted of gold evaporated onto a highly ordered pyrolytic graphite (HOPG) surface. I(V)-curves were measured for this sample on the gold surface and the HOPG surface with and without feedback for three different positions each.

The second sample consisted of gold evaporated onto an Silicon (111) surface. During the evaporation a mask of polystyrene spheres was deposited onto the Si surface and formed a two-dimensional hexagonal lattice. The mask was removed after the evaporation. Due to the fact that the gold atoms could only settle in the space between the spheres they also form a hexagonal lattice and the original size of the spheres can be determined by examining the gold structure.

All measurements were performed in the non-contact regime of the AFM.

3. Results and Analysis

3.1. Parameters of the Setup

The resonance frequency of the cantilever could be determined via the control software, which uses the method proposed by Sader [5]. A resonance curve around the estimated resonance frequency was taken (cf. fig. 3.1). Additionally to the resonance frequency, the quality factor was determined via fitting the measured curve with a Lorentzian (the quality factor is roughly proportional to the inverse FWHM of the Lorentzian) and the spring constant was determined by the program as well. They can be found in tab. 3.1. The amplitude of the excitation was chosen such that the amplitude of the cantilever was close to 1V to avoid saturation effects during the measurements.

Parameter	Value
f_R	65.75 kHz
Q	206.356
k	2.01602 N/m
A_E	0.037 V
A_R	1.006 V

Tab. 3.1.: Resonance frequency f_R, quality factor Q, force constant k, excitation amplitude A_E and resonance amplitude A_R of the system.

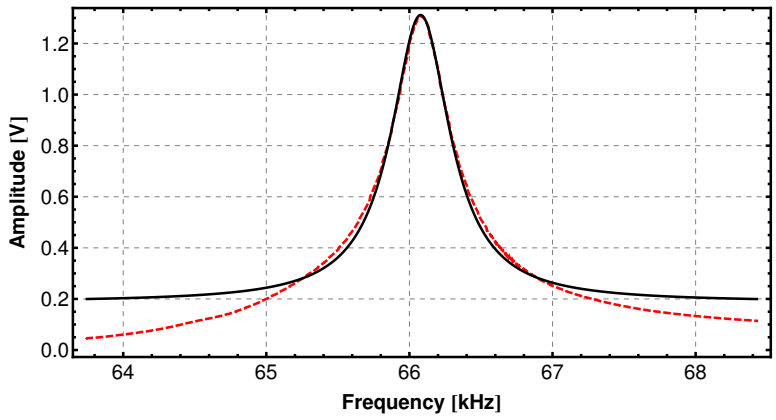

Fig. 3.1.: Resonance curve of the cantilever. The black, solid curve is the obtained data; the red, dashed line a fit with a Lorentzian shape.

3.2. Surface Topography of Au on HOPG

The topography of the sample consisting of gold islands on a highly orientated pyrolytic graphite substrate was measured for different scan sizes. Therefore a larger area for an overview of the sample and afterwards a smaller area that contained both large gold islands and graphite was chosen. Two scans can be found in fig. 3.2. Clearly visible are droplets of water on both the graphite and the gold surfaces.

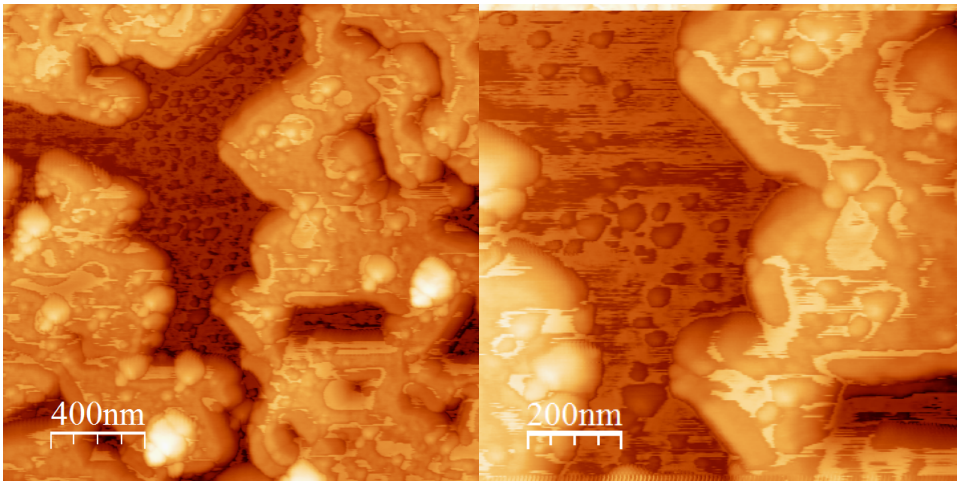

Fig. 3.2.: Gold islands on graphite. The left picture has the size $(2 \times 2\,\mu m)$ and the right is a zoom of $(1 \times 1\,\mu m)$.

3.2.1. Voltage Spectroscopy without Feedback

In order to determine the contact potential, the procedure suggested by Lü et al. [6] was used. Therefore the feedback was turned off and the amplitude of the resonance was determined in dependence on the applied bias voltage. The latter was tuned from -3 to 3V in 256 steps. Data was obtained for three spots on gold islands and for three spots on the graphite surface. The spots where chosen in such way that they were as far as possible away from the edges to graphite or gold respectively to minimize any effects due to interaction of the tip with these edges. Thereby the errors caused by the interaction of the tip with the surrounding areas were minimized. For each sample point, the data was averaged over ten measurements and fitted separately for backward and forward scanning direction and with and without regarding the interval $]-1.5\,\mathrm{V}, 1.5\,\mathrm{V}[$ due to the fact the curves show a deviation from a parabola in this region. The obtained data was fitted with MATHEMATICA using `NonlinearModelFit` with a quadratic model function

$$F_{quadr.}(V) = a\,(V + V_{CPD})^2 + b. \tag{3.2.1}$$

Comparing this with (1.4.1) shows, that V_0 is the desired contact potential.
One exemplary I(V) curve and fit can be found in fig. 3.3, the remaining data can be

found in appendix A. The obtained contact potentials are given in tab. 3.2. The given errors are obtained by the standard deviation of the numerical fit.

Position	$V_{0,\mathrm{fwd}}$ [meV]	$V'_{0,\mathrm{fwd}}$ [meV]	$V_{0,\mathrm{bwd}}$ [meV]	$V'_{0,\mathrm{bwd}}$ [meV]
Au	107 ± 4	114 ± 5	120 ± 4	126 ± 5
Au	160 ± 4	166 ± 5	151 ± 4	155 ± 4
Au	140 ± 4	146 ± 5	134 ± 4	138 ± 5
HOPG	113 ± 4	110 ± 5	102 ± 4	98 ± 5
HOPG	94 ± 4	90 ± 5	81 ± 4	78 ± 5
HOPG	94 ± 4	90 ± 4	81 ± 4	78 ± 5

Tab. 3.2.: Contact potential for three spots on gold and on graphite, measured in forward and back direction. The primed values are obtained by neglecting data points obtained at $V_{\mathrm{bias}} \in]-1.5\,\mathrm{V}, 1.5\,\mathrm{V}[$.

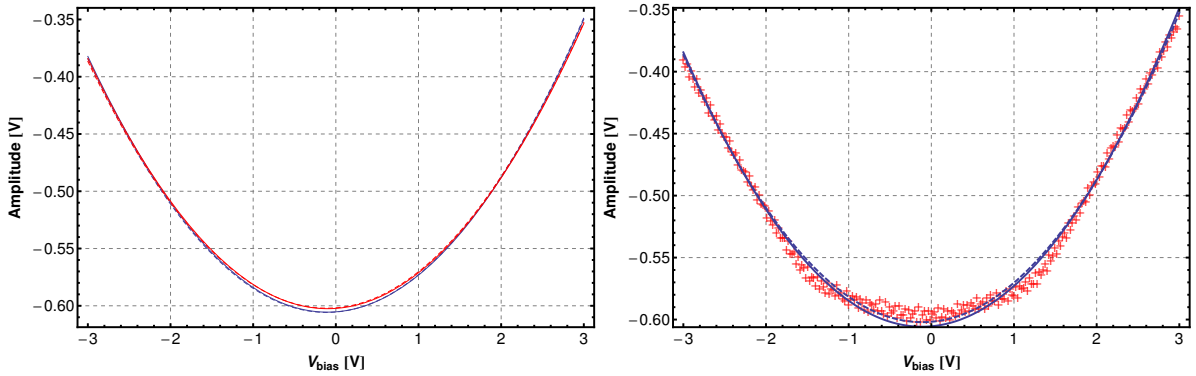

(a) Numerical fits

(b) Numerical fits with data points

Fig. 3.3.: I(V)-curve taken in no-feedback mode of graphite surfaces. (a) shows the numerical fits in backward and forward measuring direction and (b) shows the fits with the collected data. In both plots, the fits with and without disregarding the center are shown.

The contact potential is defined as the difference between the work function of the two different materials. In this case between the tip and the gold and graphite surface respectively. Due to the fact that the material of the tip is unknown, the directly obtained data cannot be compared to literature values. Nevertheless, the work function of the tip is the same for graphite and gold. Therefore the difference between the two contact potentials gold-tip and graphite-tip is taken to obtain the work function of gold-graphite, which can be compared to literature values. Taking the spread of the date presented in tab. 3.2 into account one finds a work function for gold-HOPG ranging from $-10\,\mathrm{meV}$

up to 80 meV, where the larger value is the more realistic one. Using a work function of gold of (4.83 ± 0.02) eV [7] and of HOPG in air of (4.475 ± 0.005) eV [8], one finds a value of (360 ± 30) meV. Both values differ significantly from each other.

3.2.2. Voltage Spectroscopy with Feedback

The method proposed by Olsson et al. [3] was used to determine the shape of the tip. Therefore, I(V) spectra were recorded while the feedback was turned on. This led to a constant force gradient, which can be calculated using eq. 1.3.3. Using the values as stated in tab. 3.1 and an feedback amplitude of $A = -0.6\,\mathrm{V}$ one finds

$$a = -1.67667\,, \tag{3.2.2}$$

$$\partial_z F = 1.30395 \cdot 10^{-2}\,\mathrm{Nm}^{-1}\,. \tag{3.2.3}$$

The bias voltage was tuned from -8 to 8V in 256 steps while the recorded data was averaged of 10 measurements. The recorded voltages U were converted into the sample-tip distance d via the z-calibration of the AFM

$$d(U) = 27.6\,\frac{\mathrm{nm}}{\mathrm{V}}\,\frac{U}{z\text{-Gain}}\,, \tag{3.2.4}$$

where the z-Gain value could be chosen as integer value between 1 and 15. This is necessary as the voltage control of the AFM can only manage voltages up to 10 V but the piezo has a range of up to 150 V. Thus the voltage has to be amplified by the z-Gain value to have the whole range of the piezo available. The z-Gain value set during the measurements was 15. However, the control software of the AFM has a bug and does not always take the z-Gain value into account while writing the measured data to the files, i.e. if U/z-Gain is recorded or only U. Therefore, it is not a priori clear, if the z-Gain value in (3.2.4) must be set to unity or not.

According to Olsson et al. [3] the shape of the tip is responsible for the shape of the recorded data, thus the data was fitted using MATHEMATICA's `NonlinearModelFit` using a model function of the form

$$f_{fit}[U] = f_{Olsson}[U - U_0] + c\,, \tag{3.2.5}$$

where f_{Olsson} is the appropriate function proposed by Olsson et al. (cf. tab. 3.3), c denotes an offset parameter and U_0 describes the contact potential. However, due to the fact that Olsson et al. only consider electrostatic interaction between sample and tip, the regions $[-4, 4]$ were excluded during the fitting, as this region is governed by Van-der-Waals-interaction. This can be seen in fig. 3.4, where the difference between the model functions and the measured data in the small distance regime is clearly visible.

The determined tip geometry parameters are shown in tab. 3.4. Except for the parameters calculated with an assumed z-Gain of 1, these are reasonable geometries for an AFM-tip. Using a z-Gain value of 15 as set in the control software yields also reasonable parameters for the tip geometry.

Model	Sphere	Cone	Plane
$d\|_{F'=const.}$	$\left(\frac{\pi\epsilon_0 R}{F'}\right)^{1/2} U$	$\left(\frac{\alpha^2}{4\pi\epsilon_0 F'}\right) U^2$	$\left(\frac{\pi\epsilon_0 R^2}{F'}\right)^{1/3} U^{2/3}$

$\alpha = 2\pi\epsilon_0 / \text{arcsinh}\left[(1/\tan\frac{\theta}{2})\right]$

Tab. 3.3.: Dependence of the shape of the I(V) curve on the shape of the tip. F' denotes the derivative with respect to z. (Adopted without changes from [3])

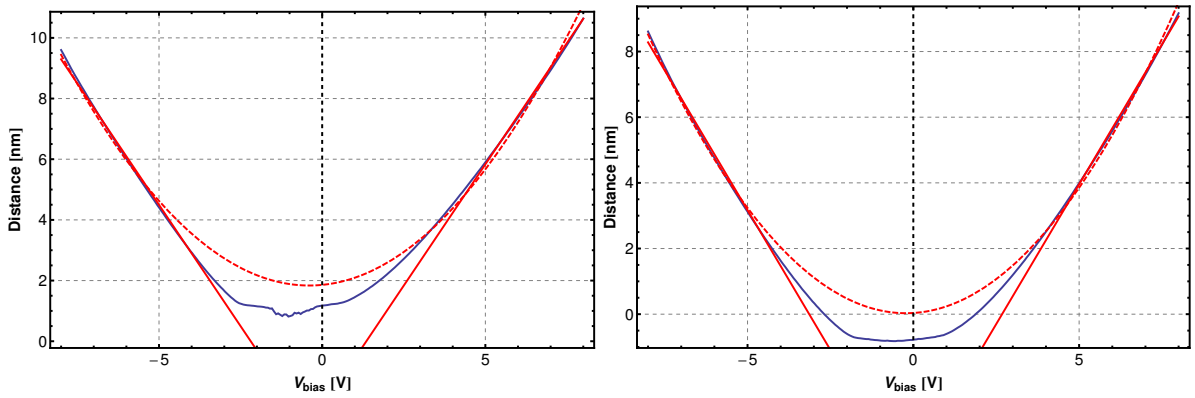

(a) Gold (b) HOPG

Fig. 3.4.: Measured I(V)-curves taken on (a) gold and (b) HOPG, where a z-Gain = 15 was used. The dashed line is the numerical fit using a Cone-tip-model and the solid line a Sphere-tip-model. The deviations of the measured data from the numerical fits due to Van-der-Waals-interaction is clearly visible. The remaining data can be found in appendix B.

Position	z-Gain	r_{fwd} [nm]	θ_{fwd} [°]	r_{bwd} [nm]	θ_{bwd} [°]
Au	1	270 ± 1	77 ± 2	270 ± 1	78 ± 2
Au	1	282 ± 1	79 ± 2	282 ± 1	79 ± 2
Au	1	299 ± 1	80 ± 2	300 ± 1	80 ± 2
HOPG	1	306 ± 1	80 ± 2	306 ± 1	80 ± 2
HOPG	1	306 ± 1	81 ± 2	326 ± 1	81 ± 2
HOPG	1	349 ± 1	83 ± 2	349 ± 1	83 ± 2
Au	10	2.68 ± 0.01	8.55 ± 0.05	$2.70 \pm .0.01$	8.55 ± 0.05
Au	10	2.82 ± 0.01	8.88 ± 0.05	2.82 ± 0.01	8.87 ± 0.05
Au	10	3.00 ± 0.02	9.32 ± 0.05	3.00 ± 0.02	9.31 ± 0.05
HOPG	10	3.06 ± 0.02	9.48 ± 0.05	3.06 ± 0.02	9.47 ± 0.05
HOPG	10	3.06 ± 0.02	9.99 ± 0.05	3.26 ± 0.02	9.96 ± 0.05
HOPG	10	3.49 ± 0.02	10.5 ± 0.1	3.49 ± 0.01	10.5 ± 0.1
Au	15	1.20 ± 0.01	4.08 ± 0.05	1.20 ± 0.01	4.09 ± 0.05
Au	15	1.26 ± 0.01	4.28 ± 0.05	1.25 ± 0.01	4.28 ± 0.05
Au	15	1.33 ± 0.01	4.54 ± 0.05	1.33 ± 0.01	4.54 ± 0.05
HOPG	15	1.36 ± 0.01	4.64 ± 0.05	1.36 ± 0.01	4.63 ± 0.05
HOPG	15	1.36 ± 0.01	4.94 ± 0.05	1.45 ± 0.01	4.93 ± 0.05
HOPG	15	1.55 ± 0.01	5.26 ± 0.05	1.55 ± 0.01	5.25 ± 0.05

(a) Tip size values calculated by numerical fits of recorded data.

z-Gain	r [nm]	θ [°]
1	304 ± 27	80 ± 2
10	3.04 ± 0.27	9.45 ± 0.68
15	1.35 ± 0.12	4.62 ± 0.41

(b) Mean values of tip geometry

Tab. 3.4.: Tip geometry values obtained by the method of Olsson et al. [3] at different assumed z-Gain values. (a) are the values obtained by numerical fits of each recorded I(V)-curve. (b) are arithmetic mean values with respect to all sets of fits, where the error is taken as the standard deviation.

In addition to 3.2.1, processing the collected data with (3.2.5) makes it possible to supplementary determine the contact potential. The value U_0 calculated via numerical fits does hereby not depend on the z-Gain. The calculated values are shown in tab. 3.5. Taking the spread into account one finds a gold-HOPG-workfunction between 40 meV and 200 meV for the parameters calculated using a Cone-tip-model and between 40 meV and 210 meV for a Sphere-tip-model. This values are considering the statistical spread in agreement with the previous findings but still too small compared with the literature value of 360 meV [7, 8].

Position	$U_{0,\text{fwd}}$ [meV]	$U_{0,\text{bwd}}$ [meV]
Au	418 ± 6	397 ± 4
Au	350 ± 6	326 ± 5
Au	344 ± 6	328 ± 5
HOPG	232 ± 6	213 ± 5
HOPG	255 ± 6	244 ± 5
HOPG	270 ± 6	279 ± 5

(a) Sphere Model

Position	$U_{0,\text{fwd}}$ [meV]	$U_{0,\text{bwd}}$ [meV]
Au	400 ± 20	383 ± 9
Au	330 ± 10	317 ± 7
Au	330 ± 10	318 ± 8
HOPG	220 ± 8	210 ± 5
HOPG	241 ± 9	238 ± 6
HOPG	250 ± 10	273 ± 6

(b) Cone Model

Tab. 3.5.: Contact potential for three spots on gold and on graphite obtained by the methode of Olsson et al. [3], measured in forward and back direction.

3.3. Surface Topography of Au on Si(111)

The second sample that was investigated was gold on Silicon. Before the gold was evaporated onto the substrate, polystyrene spheres were deposited. After the evaporation of gold, these spheres were removed and only the gold islands in between the former spheres remained on the surface, forming a hexagonal structure. Due to drifting effects of the gold atoms on the surface, this structure softened with time and gold can be found between the spots of former spheres. This can be seen in fig. 3.5.
Assuming that the spheres touched completely in the beginning, the diameter of the polystyrene spheres can be calculated from the AFM scan of the surface. A $(5 \times 5)\mu m$ and a $(2.5 \times 2.5)\mu m$ scan were taken and the gap size calculated. For this, chains of spheres in the fast scan direction were taken to minimize the error. The calculated diameter of the spheres can be found in tab. 3.6, the errors were assumed to be half the size of the gold islands between the spheres. Taking the arithmetic mean of this values yields an average of (240 ± 30) nm.

Chain	Number of spheres	Length of chain $[\mu m]$	Size of sphere $[nm]$
(a)	10	2.47 ± 0.05	247 ± 5
(b)	6	1.46 ± 0.05	243 ± 8
(c)	5	1.19 ± 0.02	238 ± 4
(d)	6	1.46 ± 0.06	243 ± 9

Tab. 3.6.: Calculated values for the size of the polystyrene spheres.

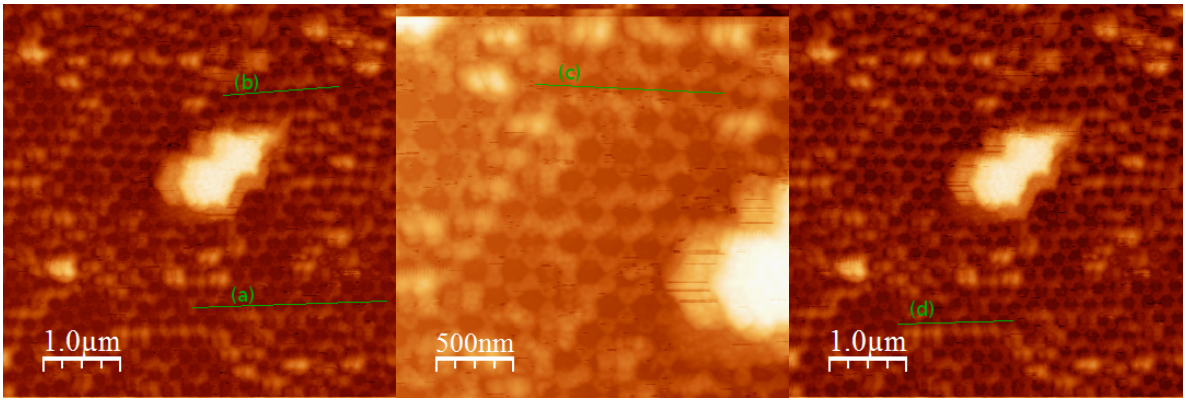

Fig. 3.5.: Gold islands on silicon, after evaporation through a mask of polystyrene spheres. The labeled lines denote the spheres that were used for the calculation of the sphere size.

4. Conclusion

The contact potential between tip and a gold surface and between the tip and the HOPG surface was determined by measuring I(V)-curves in non-contact no-feedback mode. The obtained values show a large statistical spread and therefore the gold-HOPG-work function could only be determined with a large uncertainty. This is due to the fact, that as shown in fig. 3.2 the whole surface is covered with droplets of water, which was absorbed from the ambient air. Water is a polar molecule and features a non-vanishing dipole moment. The I(V)-curves were obtained in the non-contact mode in which electrostatic forces constitute the main contribution of the forces which affect the tip. Thus, a large statistical spread is anticipated. Furthermore, the obtained value is significantly smaller than values given in the literature. This can also be explained by the unclean surface of the sample.

I(V)-curves in non-contact mode with feedback were measured as well. According to the method proposed by Olssen et al. [3] parameters of the tip geometry could be obtained. The collected data was fitted using a linear model corresponding to a spherical tip geometry and with a parabolic model corresponding to a cone tip geometry. Due to the fact, that the small distance regime of the measured data had to be excluded, neither of the tip shapes can be excluded. However, the slope of the I(V)-curves in the large distance regime can be used to exclude the plane model of Olsson et al. as they clearly do not follow a $U^{2/3}$ behavior. It has to be noted, that the models of Olssen et. al. only takes electrostatic interactions into account and is therefore a rough approximation, as e.g. Van-der-Waals-interactions are neglected. Nevertheless, the parameters determined by numerical fits for the radius of the tip $r < 10\,\mathrm{nm}$ and the cone angle $\theta < 10^\circ$ are within the expectations of a typical tip used in an AFM.

The size of the polystyrene spheres, which were used to form a mask for the evaporation of gold on silicon, could be determined directly by measuring the topography of the surface. The determined size measured via averaging over different chain lengths at different positions amounts to $(240 \pm 30)\,\mathrm{nm}$ where the error margin is determined by the statistical error of the measurement. This error also represents systematic errors due to the non-linearity of the piezoceramic tube as mentioned in 1.4.1.

Bibliography

[1] Howland, Rebecca; Benatar, Lisa *A practical guide to scanning probe microscopy*; 1st Edition; ThermoMicroscopes; 2000

[2] Martin, Y.; Williams, C.C.M; Wickramasinghe, H.K.; *Atomic force microscope-force mapping and profiling on a sub 100-Å scale*; J. Appl. Phys.; Vol. 61 (10); 4723-4729; 1987

[3] Olsson, L.; Lin, Nn; Yakimov V.; Erlandsson, R.; *A method for in situ characterization of tip shape in ac-mode atomic force microscopy using electrostatic interaction*; J. Appl. Phys.; Vol. 84 (8); 4060-4064; 1998

[4] Manual of NANOTEC AFM System

[5] Sader, J. E.; *Frequency response of cantilever beams immersed in viscous fluids with applications to the atomic force microscope*; J. Appl. Phys.; Vol. 84 (1); 64-76; 1998

[6] Lü, J.; Guggisberg, M.; Lüthi, R.; Kubon, M.; Scandella, L.; Gerber, C.; Meyer, E.; Güntherodt, H.-J.; *Surface potential studies using Kelvin force spectroscopy*; App. Phy. A; Vol. 66; Suppl. 1; 273-275; 1998

[7] Hansen, W. N.; Hansen, G. J.; *Standard reference surfaces for work function measurements in air*; Surface Science; Vol. 48; 172-184; 2001

[8] Anderson, P.A.; *Work Function of Gold*; Phys. Rev.; Vol. 115 (3); 552-553; 1959

A. Spectra for Gold on HOPG without Feedback

A.1. IV-Curves for HOPG

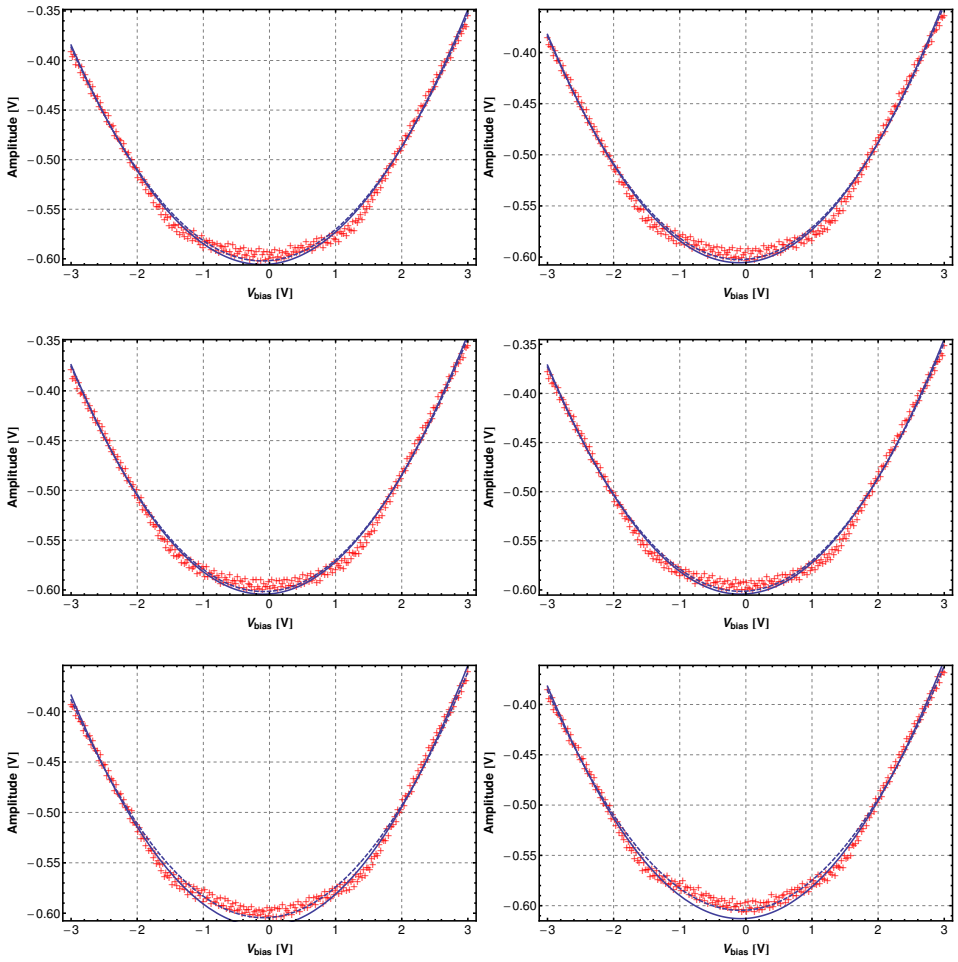

Fig. A.1.: I(V)-curves taking on HOPG surfaces at different positions. The left hand side shows the curves obtained for forward scanning direction and the right hand side for backward scanning direction. The fits are performed regarding and disregarding the center of the curves. However, this affects only the slope but not the location of the minimum and thus the contact potential

A.2. IV-Curves for Gold

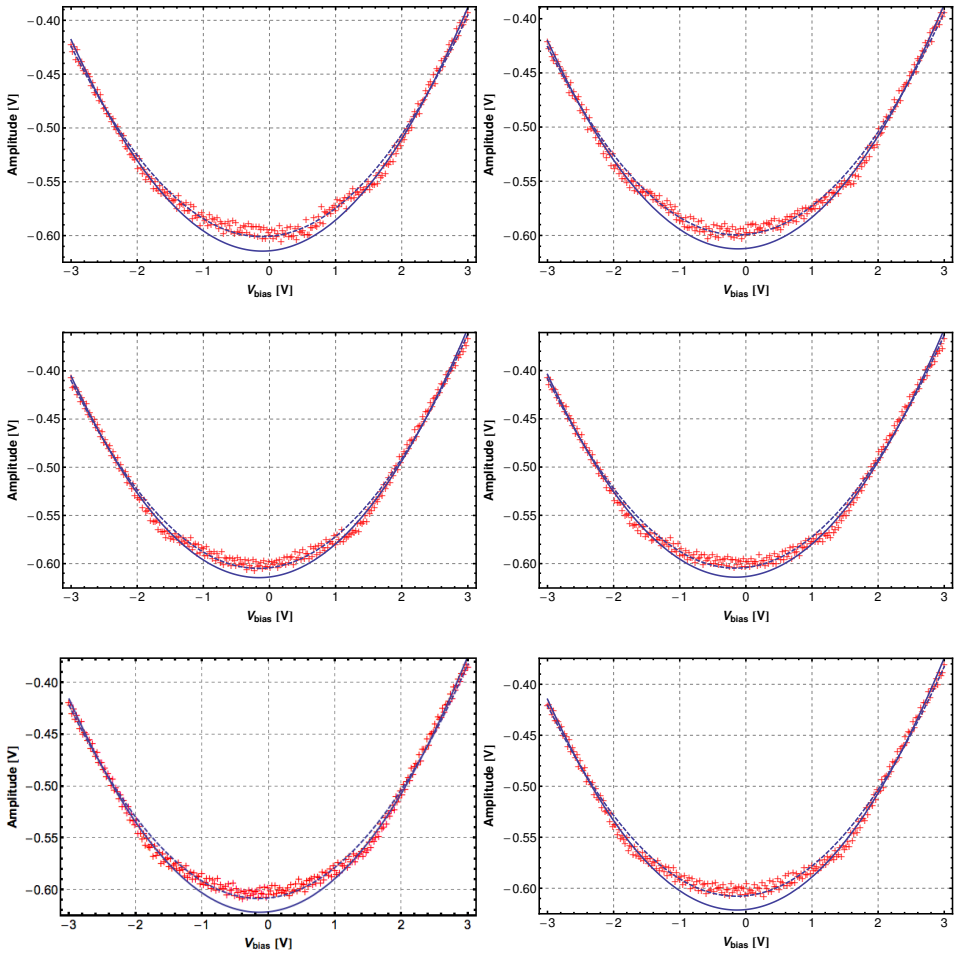

Fig. A.2.: I(V)-curves taking on gold on HOPG surfaces at different positions. The left hand side shows the curves obtained for forward scanning direction and the right hand side for backward scanning direction. The fits are performed regarding and disregarding the center of the curves. However, this affects only the slope but not the location of the minimum and thus the contact potential

B. Spectra for Gold on HOPG with Feedback

B.1. IV-Curves for HOPG

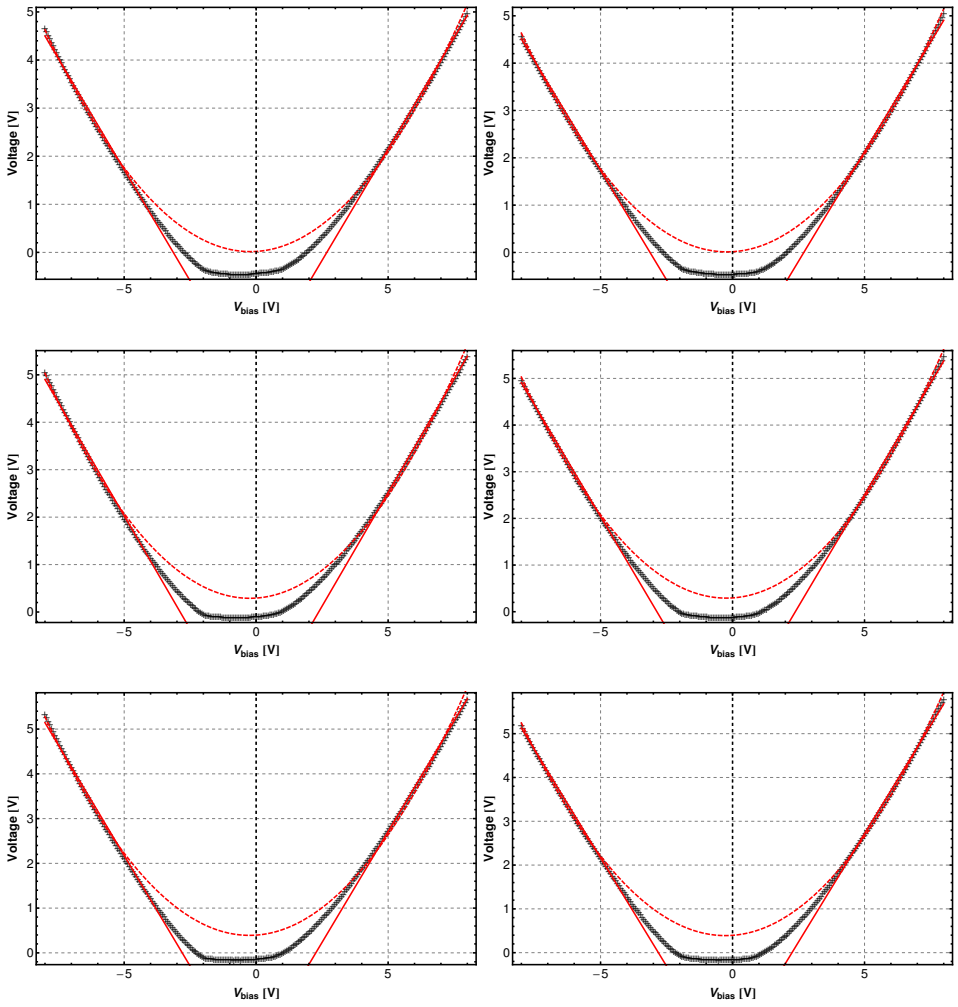

Fig. B.1.: I(V)-curves taking on HOPG surfaces at different positions. The left hand side shows the curves obtained for forward scanning direction and the right hand side for backward scanning direction. The dashed line is the numerical fit using a Cone-tip-model (parabola) and the solid line a Sphere-tip-model (straight line).

B.2. IV-Curves for Gold

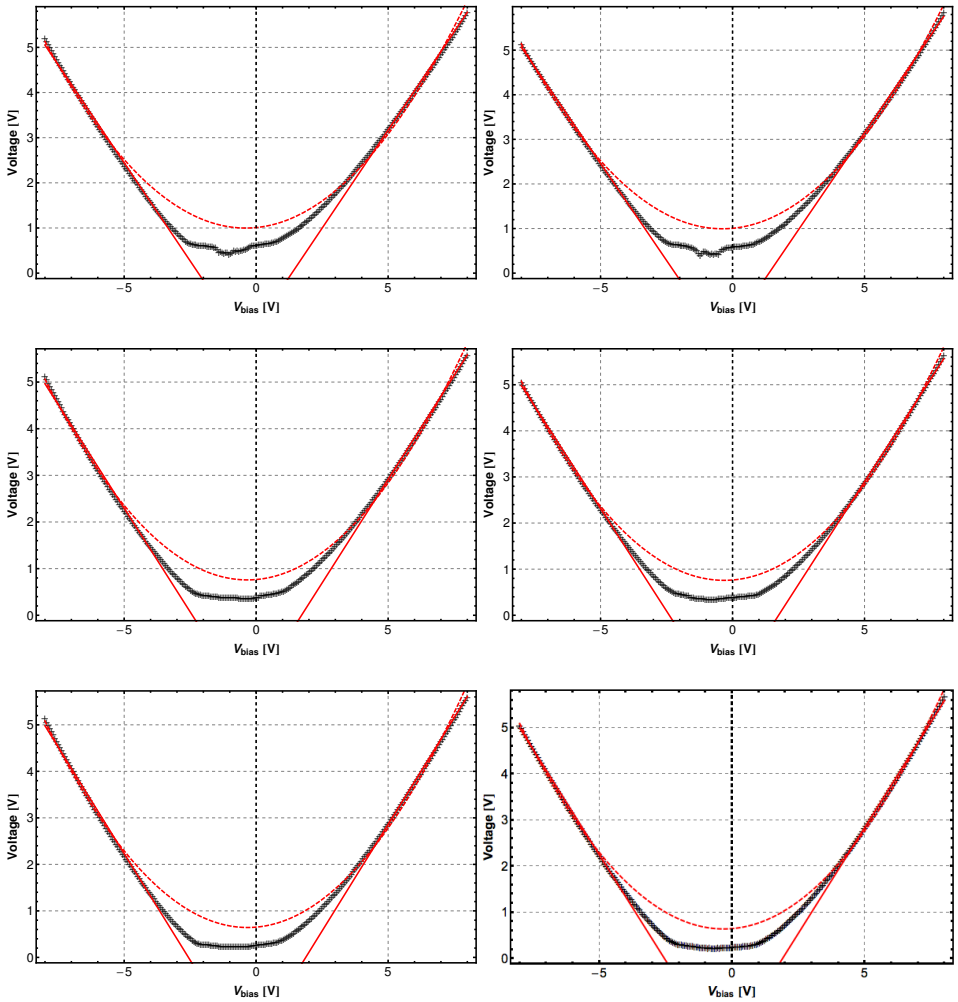

Fig. B.2.: I(V)-curves taking on gold on HOPG surfaces at different positions. The left hand side shows the curves obtained for forward scanning direction and the right hand side for backward scanning direction. The dashed line is the numerical fit using a Cone-tip-model (parabola) and the solid line a Sphere-tip-model (straight line).